Chapter 18

Techniques to Analyze sRNA Protein Cofactor Self-Assembly In Vitro

David Partouche, Antoine Malabirade, Thomas Bizien, Marisela Velez, Sylvain Trépout, Sergio Marco, Valeria Militello, Christophe Sandt, Frank Wien, and Véronique Arluison

Abstract

Post-transcriptional control of gene expression by small regulatory noncoding RNA (sRNA) needs protein accomplices to occur. Past research mainly focused on the RNA chaperone Hfq as cofactor. Nevertheless, recent studies indicated that other proteins might be involved in sRNA-based regulations. As some of these proteins have been shown to self-assemble, we describe in this chapter protocols to analyze the nano-assemblies formed. Precisely, we focus our analysis on *Escherichia coli* Hfq as a model, but the protocols presented here can be applied to analyze any polymer of proteins. This chapter thus provides a guideline to develop commonly used approaches to detect prokaryotic protein self-assembly, with a special focus on the detection of amyloidogenic polymers.

Key words Protein self-assembly, Noncoding RNA cofactor, Functional amyloid

Abbreviations

AFM	Atomic force microscopy
CF	Curve fitting
FTIR	Fourier transform infrared spectroscopy
SAXS	Small angle X-ray scattering
SRCD	Synchrotron radiation circular dichroism
TEM	Transmission electron microscopy
ThT	Thioflavin T

1 Introduction

In prokaryotes, the components of RNA metabolism self-assemble into complex structures, resulting in functional compartmentalization within the cell [1–3]. The RNA maturation components

Véronique Arluison and Claudio Valverde (eds.), *Bacterial Regulatory RNA: Methods and Protocols*, Methods in Molecular Biology, vol. 1737, https://doi.org/10.1007/978-1-4939-7634-8_18,

include proteins involved in post-transcriptional genetic regulation such as ribonucleases (RNAses) or RNA chaperone, but also small regulatory noncoding RNAs (sRNA) [2, 4, 5]. The best-characterized protein involved in such pathways using regulatory sRNA is probably the RNA chaperone Hfq [6]. Nevertheless, some others have also been identified such as ProQ and the archaeal Sm proteins [7, 8]. Our recent studies demonstrated that specific sequences in the *E. coli* Hfq C-terminus region (CTR) are able to polymerize, resulting in the formation of amyloid fibers [9]. Indeed, increasing evidence shows that amyloids are not only the result of protein misfolding associated with neurodegenerative diseases, but also found in cells for useful reasons [10]. In the later case, amyloids contribute to the physiology of the cell and are referred as *"functional"* [10]. Indeed, these functional amyloids have been widely reported in different organisms, including bacteria. In prokaryotes, diverse functions have been described for these amyloids, such as a role in biofilm development [11], formation of curli and pili [12], or creation of pores in the host membrane [13]. In this chapter we intend to provide a guideline to develop approaches that can be used to detect the fibers of sRNA protein cofactors, precisely molecular imaging, such as atomic force microscopy and transmission electron microscopy, infrared spectroscopy, synchrotron radiation circular dichroism, and small angle X-ray scattering. Our chapter will focus on Hfq and its amyloid nature as an example, but it could be applied to any self-assembling prokaryotic proteins.

2 Materials

2.1 Preparation of Samples

1. Synthetic peptide: 20 mg/mL in deionized RNA-grade water (*see* **Note 1**).
2. Purified Hfq/Sm proteins, prepared as described in the Chapter 15 by Stanek and Mura. Depending on buffer used and protein concentration reached during the purification process, the same limits apply as those described in **Note 1**.
3. UV spectrophotometer suitable for the precise determination of protein concentration measurements (micro-volumes).

2.2 Thioflavin Staining

1. ThT stock solution: 0.8 mg/mL in 10 mM phosphate buffer pH 7 containing 150 mM NaCl.
2. Fluorescence microscope equipped with a digital camera and emission/excitation filter sets to permit visualization of ThT staining.

2.3 AFM Imaging

1. AFM microscope with liquid cell.
2. AFM tips with different force constants: 2–75 N/m and resonant frequencies in the range of 100–320 kHz for imaging in

air or in the range of 0.01–0.8 N/m and resonant frequencies in the range of 70–100 kHz for imaging in solution.

3. AFM-grade mica.
4. AFM-free image analysis software such as WsXM (http://www.wsxmsolutions.com/) and Gwyddion (http://gwyddion.net/).

2.4 TEM Imaging

1. Cryo-transmission electron microscope equipped with a slow scan CCD camera.
2. Carbon-coated electron microscopy copper grid, CF200-Cu (200 mesh) or CF300-Cu (300 mesh), EMS.
3. Carbon-coated electron microscopy copper grid, ref. 01881-F (200 mesh) or 01883-F (300 mesh), Ted Pella.
4. Uranyl acetate solution: 2% (w/v).
5. Uranyl-less solution containing Gadolinium salts, Delta Microscopies.
6. Plasma cleaner.
7. Leica EM-CPC plunge-freezing device for cryo-fixation.

2.5 FTIR Spectroscopy

1. Interferometer-based spectrophotometer coupled with an IR source.
2. For transmission measurements, liquid cell equipped with CaF_2 windows and a 6 μm-thick polytetrafluoroethylene (Teflon) spacer (for example, Omni-Cell transmission Cell from Specac Company or Demountable liquid Cell from Piketech).
3. For reflection measurements, attenuated total reflection (ATR) sampling setup.

2.6 SRCD Spectroscopy

1. SRCD endstation such as that of DISCO beamline at SOLEIL synchrotron [14, 15].
2. Manually loaded circular demountable CaF_2 cells of 30 μm path length with a loading volume of 2 μL [16].
3. CDtool software for data acquisition and treatment, including averaging, smoothing, subtraction of buffer baselines from sample-spectra, calibration ((+)−camphor-10-sulfonic acid CSA), and normalization [17].
4. BestSel open access software (http://bestsel.elte.hu/) [18].

2.7 Small Angle X-Ray Scattering (SAXS)

1. SAXS beamline such as SWING at SOLEIL.
2. Quartz capillaries of 1.5 mm diameter and 0.01 mm thickness.
3. Foxtrot software (http://www.synchrotron-soleil.fr/Recherche/LignesLumiere/SWING).

3 Techniques

3.1 Analysis of Hfq Self-Assembly by Molecular Imaging

Characterization of Hfq self-assembly can be performed by microscopy techniques, including fluorescence microscopy, transmission electron microscopy (TEM), and atomic force microscopy (AFM).

3.1.1 Thioflavin Staining

Thioflavin T (ThT) is a benzothiazole salt commonly used to visualize amyloids. When bound to aggregated β-sheets, such as those found in amyloids, the dye displays an enhanced red-shifted fluorescence emission spectrum [19]. Even if the dye fluorescence is not completely specific and may bind to other structures (such as double-stranded DNA), it is however a good indicator that amyloid structures are formed in the sample. Practically, for ThT staining:

1. Dilute protein samples to 0.2 mg/mL.
2. Prepare a stock solution of ThT. This solution can be filtered and stored in the dark for 1 week. Before use, the stock solution is diluted in 10 mM phosphate buffer pH 7 containing 150 mM NaCl (dilution 1/50 = working solution); this must be done extemporaneously.
3. For a spectroscopic assay, add a 10 µL aliquot of protein to 1 mL of working solution, incubate for 1 min, and measure the fluorescence intensity with excitation set at 440 nm and emission detected in the range 450–500 nm (*see* **Note 2**).
4. For slide staining and visualization under a microscope, place 10 µL aliquots of stained samples and image using a fluorescence microscope with a 60× oil-objective (NA = 1.4). The laser excitation can be set at 415 or 450 nm and emission is detected at 482 nm.

3.1.2 AFM Imaging

Atomic force microscopy (AFM) has become a common tool for the analysis of protein aggregation and fibrilization [20]. It provides height information that complements structural information from two-dimensional projection images obtained using electron microscopy (*see* Subheading 3.1.3). In essence, an AFM setup consists of a microtip attached to a cantilever held on a piezo scanner that moves along the surface of the sample with high precision over a defined distance within the micrometer range. The deflection of the cantilever follows the surface topography and is monitored following the position of a laser spot reflecting from its surface on a photodiode. The motion of the cantilever can also be used to interrogate the mechanical properties of the sample. AFM imaging thus provides information about biological objects dimensions at nanometer resolution [21]. As amyloid fibrils are usually in the µm range in length with a lateral dimension between 3 and 30 nm, AFM is thus perfectly adapted to probe fibrils structure.

1. Substrate preparation. In order to study fibrillar protein structures, it is essential to first adsorb them to a flat surface.

This step is crucial for obtaining high-quality data. The fibers formed in solution have to be at an adequate density and firmly attached to allow the tip to scan over them. One of the surfaces that is most frequently used for AFM studies is mica, although clean glass or annealed gold can also be used. Here we will concentrate on describing the adsorption of fibrils to mica surfaces. Mica is convenient because it is atomically flat and can be easily cleaved immediately before use to obtain a clean surface. AFM-grade mica can be easily obtained from several AFM product suppliers. The freshly cleaved mica is glued to the sample holder using, for example, double-sided tape before incubating the protein sample.

2. Protein adsorption. A protein solution is incubated on the mica surface to allow for fibril adsorption to the surface (*see* **Note 3**). The size, charge, and mechanical stability of the fibers determine the details of the preparation protocol. Basically this protocol consists of two steps: first, conditioning the surface where the fibers will be deposited and second, incubating the protein solution to allow for filament deposition. As the surface/protein interaction will be affected by the surface charge of the protein and surface, the pH of the solution has to be selected to optimize this interaction. Precisely, mica is constituted of sheets of octahedral hydroxyl-aluminum lying between two silicon tetrahedral layers. The most favorable cleavage plane is located in the layer of unbound K^+ that lies in the interlayer space between neighboring silicon layers. When immersed in water, the hydrated potassium ions can be dissociated from the mica surface, leaving negatively charged aluminum tetrahedra (AlO_2^-) in the first outer layer [22]. Thus, the solution pH and ionic salt concentration should be adjusted to allow for the protein to be positively charged to promote its interaction with the negatively charged mica surface.

3. Imaging in air. If the protein binding to the surface is not strong enough to allow imaging with the sample immersed in solution, the best alternative is to image in air. Incubate a small amount of diluted protein (typically 10 μL of 5–10 μg/mL fibrils) on the mica surface and allow to air dry at room temperature. All the fibers in the solution will now be adsorbed on the mica surface. Before imaging, the sample must be extensively washed with Milli-Q water to remove the salt from the buffer and then carefully air-dried again. AFM can operate in different modes, and the ones more conveniently used to image amyloid self-assemblies are contact mode and tapping mode, depending on the characteristics of the fibrils of interest [21]. Contact mode images are obtained when the tip is in contact with the sample, so it requires that the fibers are firmly attached to the surface and rigid enough to withstand the tip

pressure as it scans along the surface without deformation or sliding. In tapping mode, the cantilever is oscillated at its resonant frequency during the scan, so that it does not drag the sample along as it moves over the surface. Resonant frequencies of the soft cantilevers used for biological materials are, typically, within the 70–100 KHz range, depending on whether the microscope is operated in air or in solution, so that the interaction time between the tip and sample is reduced dramatically to only a few microseconds. Fibers can be imaged either in tapping or in contact mode, depending on the characteristics of the sample.

4. Imaging in solution. If the fibers are sufficiently long and their interaction is strong enough to allow for a stable adsorption to the surface, the fibers will remain firmly attached during imaging in solution. After allowing 10–60 min of incubation, the sample is extensively rinsed with buffer to remove excess protein. The imaging buffer is selected to optimize the interaction between the tip and the sample and could differ from the one selected for fiber adsorption to the mica. The pH or salt concentration can be adjusted again so that the tip–protein interaction is minimized to reduce damaging the fibers during imaging. Operating in solution offers the possibility of imaging fiber growth. In such a case, imaging should be done in the presence of small amounts of protein in the solution to avoid interfering with the imaging process. Images of the same area taken at different times can be used to follow filament growth kinetics.
5. AFM imaging procedure. Once the sample is properly prepared, the AFM is operated selecting the most appropriate tip for the imaging mode. If imaging in air, stiffer tips with force constants in the range of 2–75 N/m and resonant frequencies in the range of 100–320 kHz can be more convenient to reduce the snap-to-contact region. For imaging in solution, softer tips, with force constants in the range of 0.01–0.8 N/m and resonant frequencies in the range of 70–100kHz can be used. In brief, AFM operation includes the following steps: placing the cantilever in the holder and then both to the scanner; aligning the laser to impinge the cantilever tip; aligning the laser reflection on the center of the photodiode; placing the sample in the sample holder; if operating in tapping mode, the cantilever resonance frequency has to be selected; approaching the tip and sample. Once the tip is touching the sample, the scanning parameters, gains, scanning speed, and setpoint, are adjusted to obtain reproducible trace and retrace images.
6. AFM topographic analysis. AFM obtains direct topographical images of the sample surface. Each AFM provider includes software to analyze the images, but there are also free specialized

software available to process scanning probe microscopy images (WsXM or Gwyddion).

Figure 1a–f shows Hfq peptide fibers imaged in air or in solution.

3.1.3 TEM Imaging

A quick way to check the presence and structural characteristics of fibers (length, diameter, interweaving), as well as the homogeneity of the sample, is negative staining and observation by transmission electron microscopy.

Protocol for Negative Staining

1. Sample preparation. Deposit a 5 μL drop of Hfq sample at 1 mg/mL in 50 mM phosphate buffer pH 7 (i.e., stock solution diluted in water) on a glow-discharged carbon-coated electron microscopy copper grid (200 mesh square grid, EMS). In order to optimize the adsorption of the sample to the grid it is recommended, but not strictly required, to realize a glow-discharge (gas ionization process giving the carbon film hydrophilic).

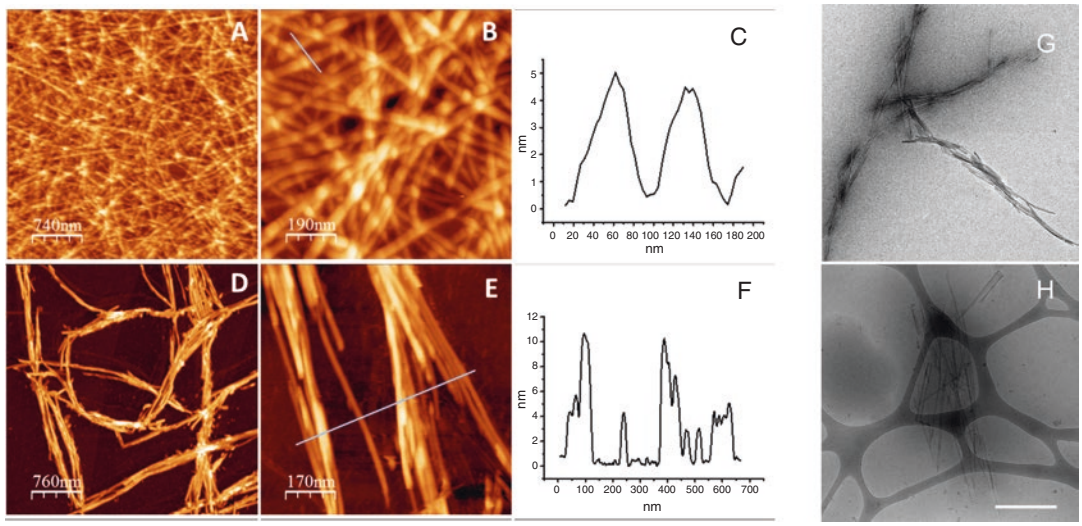

Fig. 1 Visualization of Hfq self-assembly by molecular microscopy. Transmission electron microscopy (TEM) and atomic force microscopy (AFM) are efficient tools to investigate protein nanostructures. (**a**–**f**) AFM images of Hfq peptide fibers in air and under liquid. Upper panels (**a**, **b**, **c**) are fibers imaged in air. A drop of the protein solution was allowed to dry on the mica before imaging in contact mode. Lower panels (**c**, **d**, **f**) show filaments observed under buffer at pH 4 in tapping mode, after incubating the fibers for 5 min on mica at pH 4 at a concentration of 0.5 mg/mL. Panels C and F show the height profile under the blue lines shown, respectively, in panels **b** and **e**. (**g**–**h**) In TEM experiments, 5 μL of Hfq solution is deposited on a glow-discharged electron microscopy grid covered by a continuous carbon film for negative staining (**g**) or a holey carbon film for cryo-TEM (**f**). (**g)** The sample is dried and subsequently stained with a solution of either uranyl acetate or uranyl-less (filling the protein cavities with heavy atoms). (**h**) The excess of sample is blotted and subsequently frozen in ethane at liquid nitrogen temperature (embedding the sample in thin amorphous ice layers). Both methods show filaments that seem more aggregated in negative staining. *Scale bar:* 500 nm

2. Sample adsorption. After 5 min of interaction, blot out the excess sample using a Whatman filter paper (1–3 min is usually enough to have efficient adsorption of the sample onto the grid).
3. Contrasting of the sample. The adsorbed sample can then be put in contact with the contrasting agent. To perform negative staining, 5 μL of uranyl acetate solution (2%) is applied onto the grid-containing sample. After 30 s incubation, the excess of uranyl acetate is blotted out and then the grids can be kept in a dry dark dust-free environment until observation at the electron microscope. Gadolinium salt (uranyl-less) is also used for negative staining. It is used instead of uranyl acetate because it is safer. However, it may create artifacts such as crystals. Store it at cold temperature and use it at room temperature to avoid salt deposition as much as possible.
4. The grids can be stored at room temperature for further observation on any standard transmission electron microscope.
5. Sample observation. The electron microscopy grid is then mounted onto a room temperature-equilibrated holder and subsequently introduced into an electron microscope (JEOL 2200FS, JEOL, Tokyo, Japan).
6. Image acquisition. 2 k by 2 k images are acquired using a Gatan Ultrascan 894 US1000 slow scan CCD Camera (Gatan, Pleasanton, CA, USA) at 40,000× nominal magnification (corresponding pixel size was 0.32 nm).

Figure 1g shows Hfq peptide fibers imaged by TEM after negative staining.

While it is true that negative staining is the tool of choice for quick characterization, it implies the dehydration of the sample, which can lead to artifactual aggregations of fibers or to structural modifications. Therefore, when high-resolution ultrastructural studies are required, samples should be observed in hydrated conditions, which is possible by cryo-transmission electron microscopy (cryo-TEM). Cryo-TEM is based on fast-freezing of the electron microscopy grid containing a thin layer (100–200 nm or less) of the adsorbed sample by quick immersion in liquid ethane cooled-down at liquid nitrogen temperature. This can be achieved by using a lab-made or commercial apparatus. Some commercial apparatuses can be fully automatized so that repetitiveness can be easily achieved when freezing conditions have been set up.

Protocol for Cryo-Electron Transmission Microscopy (Cryo-TEM)

1. Sample preparation. Deposit a 5 μL drop of Hfq suspension on a glow-discharged lacey carbon film grid (300 mesh).
2. Sample freezing. Blot the suspension through the grid for about 1 s using a Whatman filter paper to create thin suspended films in the carbon holes of the grid. Using a Leica EM-CPC, plunge

the grid into liquid ethane cooled-down with liquid nitrogen. Prior to sample freezing, the grid is kept in a liquid nitrogen storage unit until observation at the electron microscope.

3. Transfer to the electron microscope. The grid with the frozen hydrated sample is transferred to a cryo-TEM for observation. During this transfer process, and during observation, the sample should remain under liquid nitrogen to prevent water crystallization, which impedes the observation of the sample. Since the observed sample is fully hydrated, the obtained images reflect the near native structure of proteins and fibers. A simple but detailed description of negative staining and cryo-TEM techniques is described in [23]. Grids are transferred into a JEOL JEM 2200FS cryo-electron microscope equipped with a Ω-energy filter by using a Gatan 914 cryo-transfer system.
4. Image acquisition. Hfq peptide cryo-images can be acquired using a 2 k by 2 k Gatan Ultrascan 894 US1000 slow scan CCD Camera (Gatan, Pleasanton, CA, USA) at 40,000× nominal magnification (corresponding pixel size was 0.32 nm) with an energy window of 20 eV.
   Figure 1h shows Hfq peptide fibers imaged by cryoTEM.

3.2 Analysis of Hfq Amyloid-like Self-Assembly Secondary and Super-Secondary Structure

3.2.1 Infrared (FTIR) Spectroscopy

Fourier transform infrared (FTIR) spectroscopy can be used to analyze protein secondary and super-secondary structures such as amyloid. The peptide bond is an amide group (CONH) that gives rise to seven active absorption bands in the infrared. This method can thus give information on secondary structure (three bands carry information on the secondary structure, but the Amide I band is the most used, see below) and tertiary structure (through the Amide II band). Indeed, the Amide II spectral region studied in the presence of D_2O solution (i.e., Amide II′, *see* **Note 4**) is a marker of the partial opening of the protein and thus of the tertiary structure changes, during which the hydrogens remained within the protein core undergo H-D exchange [24]. The Amide I is most often used for secondary structure elucidation since it has the smallest contribution from peptide side chain absorptions. The Amide I band absorption is mainly due to the C=O stretching of the amide group vibration but this vibration is strongly delocalized over the amide C–N and C–H bonds giving rise to a strong coupling: the trans dipole coupling. The exact frequency of the absorption peak is thus sensitive to the angle of the amide bond, which is dependent on the local structure of the protein domain. α-Helices, β-sheets, β-turns, random coils, and 3–10 helices are each restricted to a different set of angles as seen in a Ramachandran plot, giving rise to amide peaks located at different frequencies. This gives rise to the sensitivity of infrared spectroscopy to the secondary structure

of proteins. Here, we thus focus on the infrared zone in the region of the Amide I.

1. Hfq fibril samples (from 1 to 20 mg/mL) are loaded into liquid cell equipped with CaF_2 windows and a 6 μm thick spacer. This configuration allows studying a sample in solution for several hours (8 on average), and therefore allows for following the aggregation kinetics.
2. FTIR absorption measurements are performed between 1000 and 4000 cm^{-1} through the use of an interferometer-based spectrophotometer coupled with an IR source and a Triglycine sulfate (DTGS) detector. The best way to have good transmission spectra is by performing a measurement in which 256 scans are collected and at least 5 independent measurements are averaged. Spectra at a nominal resolution of 2 cm^{-1} are baseline corrected and background subtracted before analysis. A spectrum of the buffer must be collected using the same experimental parameters for water subtraction. Buffer subtraction is performed by an iterative procedure to remove the signal originating from the water. The association band of water between 1800 and 2400 cm^{-1} is used to compute the subtraction factor. Most commercial software packages propose an integrated subtraction routine.
3. Alternatively, an attenuated total reflection (ATR) sampling setup can be used. With an ATR setup, the infrared beam light is reflected inside an infrared-transparent, high refractive index crystal. The crystal can be single bounce or have a multiple bounce geometry to increase sensitivity. An evanescent wave is created at the crystal–solution interface, which extends into the sample with a penetration depth typically around 1 μm (depending on the wavelength and on the crystal's refractive index). A background spectrum without sample is first recorded. A total of 64 scans are usually averaged. Then, ~ 5–20 μL of fibril sample (1–20 mg/mL) is deposited directly on the crystal and covered with a cap to reduce evaporation. A spectrum of the buffer must also be recorded in the same conditions for latter subtraction.
4. The analysis consists of qualitative evaluation of secondary structure through the combination of 2nd-derivative, Fourier self-deconvolution (FSD), and curve-fitting (CF) analysis [25]. FSD and the 2nd-derivative can be used to find the number and exact positions of the overlapping peaks composing the Amide I band. CF involves fitting a series of model peaks to the experimental data. The best function for peak shape in liquid samples is usually a convolution of Lorentzian and Gaussian bands, the Voigt profile. Overlapping peaks composing the Amide I band are fitted with Voigt profiles with a bandwidth

varying between 15 and 25 cm^{-1}. The goodness-of-fit is generally evaluated by comparing the rest with the noise. The CF, being an iterative algorithm, is pursued until the rest is less than 5 times the noise. The integration of the area of the component bands used to generate the final curve fit can provide an estimate of the relative percentages of secondary structure present. Both qualitative and quantitative analyses can be achieved with dedicated software. Most software packages such as OMNIC™ (Thermo Fisher Scientific) and Opus (Bruker) provide curve-fitting algorithms.

5. The assignment of a peak at a given wavenumber to a given secondary structure should be done according to Table 1. Briefly, a peak near 1645 cm^{-1} is indicative of random coil, 1655 cm^{-1} of α-helix, and 1630 cm^{-1} and 1690 cm^{-1} of β-sheet (*see* **Note 5**). Stronger hydrogen bonding results in a shift to lower wavenumbers and, therefore, amyloid fibrils often have β-sheet peaks below 1630 cm^{-1} [26].

Figure 2a shows Hfq peptide fibers analyzed by FTIR spectroscopy.

3.2.2 Synchrotron Radiation Circular Dichroism SRCD

Circular Dichroism (CD) is a sensitive absorption spectroscopy technique for studying biological samples such as proteins and polynucleotides (DNA and RNA) as well as sugars. Circular left and right polarized light is differentially absorbed, e.g., by proteins due to the excitation of the n-π and π-π* electronic transition of the peptide bonds. Additionally the aromatic side chains produce characteristic absorptions between 210 and 275 nm. Standardized CD spectra can be deconvoluted and used for protein secondary

Table 1
Empirical assignments for Amide I infrared (IR) bands characteristic of proteins [25]

Wavenumber (cm^{-1})	Assignment
1615–1625	Intermolecular β-sheet (in particular vibrations of strongly bound intermolecular aggregated β-strands, including amyloids)
1630–1640	Intramolecular native β-sheet
1640–1650	Disordered random coil
1650–1660	α-Helix
1660–1695	β-turn
1675–1695	Intermolecular β-sheet (in particular antiparallel aggregated β-sheets)

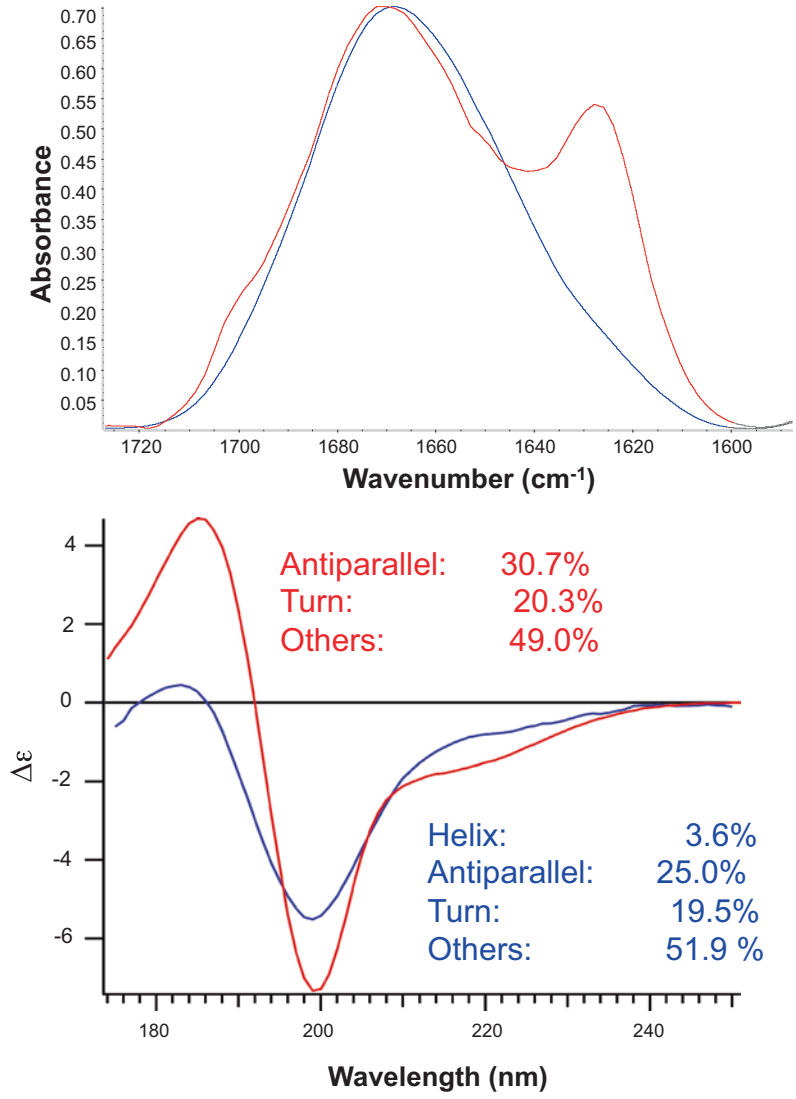

Fig. 2 Secondary and supersecondary structure determination. (**a**) FTIR spectra of Hfq peptide immediately after diluting in water (blue) and after incubation for 1 day at 20 °C (red). The peaks shown in (**a**) are due to intermolecular aggregated β-sheet at 1620 cm^{-1} and to the presence of native β-turn at 1670 cm^{-1} and intermolecular aggregated β-sheet at 1690 cm^{-1}, respectively. In addition, in a lot of proteins studied, the contemporary increase of the components at about 1620 and 1680 cm^{-1} indicates the building of antiparallel β-aggregated structures; the low frequency β-sheet moiety at approximately 1620 cm^{-1} are attributed to multistranded intermolecular β-sheet and resembles the typical fingerprint of the cross-β motif found in amyloid-like fibrils [37, 38]. (**b**) SRCD spectra of Hfq peptide at 20 mg/mL in water (blue) or after incubation at 20 °C for a few days at 100 mg/mL to ensure the formation of fibrils (red). In this case, sonication procedure to fragment fibrils into shorter forms or their monomeric form was not necessary. Secondary structure determination by BESTSEL (inset) revealed a structural increase of 5% in β-sheet content for the fibrils as opposed to the monomeric Hfq peptide

structure determination. Synchrotron radiation circular dichroism (SRCD) allows for the extension of the spectral range down to 168 nm in aqueous solution and 120 nm in hydrated films, with very good signal-to-noise ratios (typically ~20 mdeg/0.2 mdeg). The extension of the spectral range down to 168 nm has improved the information content obtainable from a SRCD spectrum. Especially for the weak CD signals of proteins with high β-sheet or disordered content, SRCD has improved the spectral analysis substantially [27]. Numerous algorithms exist for the estimation of the secondary structure composition from CD spectra. For the special case of β-sheet-rich proteins, with a broad range of protein folds, a recent publicly accessible algorithm BestSel [18] allows the determination of secondary structure contents including parallel and antiparallel β-sheets and potential fold recognition. The novel reference dataset with spectra that significantly differ from present reference sets extends the information content for secondary structure determination.

1. Sample preparation. Homogenized Hfq peptide fibrils were prepared by diluted peptide in water at 20 mg/mL to 100 mg/mL. Observation of fibrils can be made directly after few days (*see* **Note 1**) as described in **step 5**. Nevertheless, in some cases long and associated fibrils need to be fragmented to shorter and individual pieces to be analyzed, as described below (2–4).
2. Seeds can be prepared by a sonication procedure [28]. The sonication strength and time had to be carefully chosen. At low force, homogenization of the fibril solution will just decrease the viscosity by breaking the fibrils into shorter pieces. A microtip sonicator set up in the cold room needs to be regulated to minimal strength (force, amplitude), with a 50% duty cycle (e.g., 1 s pulses interrupted by 1 s silence). Sample volume should be at least 100 μL in microtubes. Sonication shall be carried out with the tubes containing sample cooled in ice-cold solution (for better contact), with the tip plunged right to the bottom of the tube without touching the tube wall. For homogenization of peptides and small proteins four cycles of five pulses with a 10 s rest between cycles produces reliable and reproducible results. During the rest period, mix well the solution containing the peptide by lifting and plunging the tip up and down. Droplet formation on the tube wall should be avoided. Gloves, mouth mask, and glasses are recommended for safety.
3. SRCD spectra are taken before and after sonication allowing the spectral distinction between fibril seeds and amyloid fibrils.
4. Ultracentrifugation in Beckmann TLA-100 rotor run at 53500-96500 Relative Centrifugal Field (RCF) × g for 15–30 min may be used to distinguish eventual monomers floating in the supernatant and the fibrils accumulating in the

pellet. The baseline spectrum for the fibril seeds should be taken from the supernatant. Once the sonication and centrifugation are finished, keep samples at 4 °C.

5. Sample concentration, buffer composition, and pathlength choices for SRCD data acquisition should be handled with care. In general, concentrations should be for α-helix rich proteins 1–2 g/L, for β-sheet rich proteins 3–4 g/L, and for unordered structures above 5 g/L in a 20 μm pathlength cell. Loading volumes are 2 microliters in special 20 μm CaF_2 cells [16] (Fig. 3). The choice of buffer is a function of how much chloride will be considered essential (10–50 mM NaCl allows obtaining spectra down to 185 nm). Chloride is readily replaced by fluoride allowing twice the initial chloride concentration. Ideally phosphate buffer is used being more temperature stable than Tris-Cl and being deep-UV transparent.

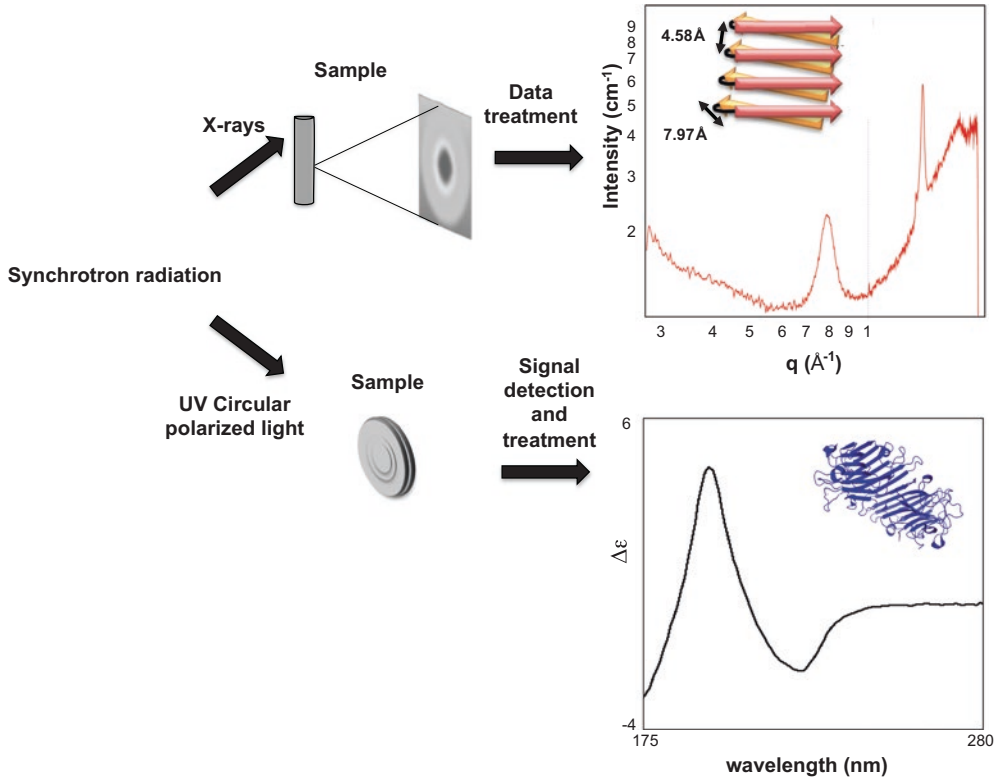

Fig. 3 Use of synchrotron radiation for the analysis of amyloids self-assemblies. Top: Basic sketch of data acquisition and treatment at a SAXS beamline. The sample scattering pattern recorded by a 2D detector is radially averaged to and background is subtracted to give the following SAXS curve. The CTR peptide of the Hfq protein exhibits typical diffraction peaks corresponding to a cross-β structure sketch in overlay. Bottom: Data acquisition and treatment at a SRCD beamline. A rich **β**-strand containing protein is shown as an example (Concanavalin A, PDB ID 4PF5 [39])

6. All spectra are normalized to the mean residue weight ellipticity (Θ_{MRW}, deg.cm^2.dmole^{-1}).
7. For secondary structure determination with BestSel, normalized root-mean-square deviation (NRMSD) indicates the most accurate fit for each spectrum; values of <0.15 are considered significant.
   Figure 2b shows Hfq peptide analyzed by SRCD spectroscopy.

3.3 Characterization of Cross-β Structure

Small angle X-ray scattering (SAXS) is a simple and powerful technique that directly provides structural information at scales ranging typically from 1 nm to 1 μm [29–31]. The physical principle is the same as X-ray crystallography; it is based on elastic scattering of an incoming X-ray wave by the electrons of the sample. The resulting "signal" is a scattering pattern most frequently collected using a bi-dimensional detector positioned behind the sample and perpendicular to the incoming beam. Practically, SAXS experiment can bring information for either peptides in solutions or assembled materials made of peptides. In this section, we will focus on how to prepare and analyze amyloid peptides and particularly Hfq cross-β structure.

3.3.1 Sample Preparation

1. Different solutions of peptide are prepared (25–100 μL), ranging from 0.5% w/v to the highest concentration by 2.5% steps by dissolving the peptide into an appropriate buffer. The buffer must be the same for the previously described experiments (FTIR, SRCD…) in order to compare the results; buffer containing phosphorous should be avoided and low salt concentration is better.
2. When all the solutions are ready, directly fill quartz capillaries of 1.5 mm diameter and 0.01 mm thickness. Then, capillaries are sealed using wax or nail polish. The capillaries containing the peptides are left at room temperature until cross-β strands are obtained (this is usually determined by other methods).
3. If the cross-β strand formation kinetics are unknown, FTIR will be a better method than SAXS to determine the kinetics of assembly.

3.3.2 SAXS Setup and Recording

The SAXS experiment can bring information for both peptides in solutions or assembled materials made of peptides. The intensity collected is proportional to the number of objects within the sample, *N*. It directly results from their size, shape, and internal structure, given by the Fourier Transformation modulus of their electronic density, showed here for an isotropic sample:

$$I(q) = r_e^2 \sum_{p=1}^{N} \left\langle \left| \iiint_{V_p} \left(\rho_e(\vec{r}) - \rho_0 \right) e^{-i\vec{q}\cdot\vec{r}} d^3r \right|^2 \right\rangle_\Omega$$

where the triple integral is performed within the volume V_p of each particle and the average performed over all possible orientations Ω. r_e is the classical electron radius, $\rho_e(\vec{r})$ is the electronic density at position $\vec{r}$ within the particle, ρ_0 is the average electronic density of the surrounding buffer, $q = \frac{4\pi \sin\theta}{\lambda}$ is the momentum transfer, θ is the scattering angle, typically below a few degrees, and λ is the X-ray wavelength. The rotational average severely limits the structural information content of the scattering pattern for a non-assembled material obtained in a SAXS experiment. When isolated macromolecules assemble into regular structures, new correlations appear in the electronic density of the whole structure, giving rise to specific modulations in the scattering intensity. When motifs are repeated along a defined axis with a repetition distance d, the scattered photon waves undergo strong constructive interferences at q values given by $q = n\frac{\pi}{d}$, where n is an integer (Bragg law). The phenomenon is called diffraction, but is not different in nature from solution scattering. When identical units, e.g., a peptide or a protein, are regularly spaced, with periodicities typically on the order of or larger than 1 nm, diffraction is observed in the Small angle range (SAXD) [32].

1. Cross-β structure is investigated here. The sample-to-detector distance needs to be optimized. The typical signals resulting from β-sheet structure correspond to inter-distances of around 10 and 4.7 Å; the available q-range should thus be from 0.3 to 2 $Å^{-1}$.
2. Capillaries containing the samples and buffer (control) are mounted onto capillary holder system and positioned into the beam path.
3. Depending on the sample homogeneity, several positions within the sample capillaries can be chosen. At least 3 positions are enough: one at the top of the sample, one in the middle, and the last at the bottom.
4. One important step here is the detection of radiation damage. When exposed to X-rays, organic molecules tend to form free radicals, leading to aggregation of the sample onto the capillary wall. Radiation damage does not occur for all samples. This phenomenon is observable after data treatment by an increase of the curve intensity at small q. In order to avoid this problem, samples should be exposed to X-rays and then let to rest for a few seconds before a new exposition at the same spot.
5. As samples on the same capillary holder can vary greatly, the exposure time must be adjusted, in order to get enough signal and to avoid saturation on the detector (depending of the beamline detector).

6. Due to radiation damage, acquisition time should not be higher than 3 s with at least 5 s of pause. It is better to make 10 acquisitions of 3 s than 1 of 30 s.
7. Record the scattering pattern with short and identifiable sample and buffer names.

3.3.3 Data Treatment

1. When the entire scattering patterns are recorded as 2D images, radial integration is performed in order to obtain SAXS curves for each position inside all the samples and buffers. Such operation can be done using the Foxtrot software or equivalent.
2. For curves corresponding to the same position within the same sample, averaging is suggested in order to obtain better statistics. This must be done carefully in order to avoid averaging data with radiation damage.
3. As samples are analyzed within the buffer, the buffer signal needs to be subtracted. Data subtraction is provided by most of the SAXS data reduction software.
4. When the resulting final curve (averaging + subtraction of buffer) is obtained, diffraction peaks corresponding to cross-β sheets should be observed. The example of Hfq C-terminus peptide is shown on Fig. 3 (top), where the anisotropic reflections are indicative of a partially aligned fiber, perpendicular to the X-ray beam. The reflections at d = 4.58 Å and d = 7.97 Å correspond, respectively, to the inter-strand and inter-sheet spacing.

4 Concluding Remarks

The self-assembly of biological macromolecules constitutes a key process in all living organisms. We recently reported that sRNA cofactor Hfq belongs to the family of functional amyloids [9]. The various experimental approaches described in this chapter aim at further investigating the self-assembling properties of sRNA cofactors. This could indeed represent a versatile means to regulate sRNA-related processes in vivo. Furthermore, this would also enable the formation of mixed synthetic sRNA:protein synthetic self-assemblies, with future perspectives for nanotechnologies.

5 Notes

1. The main obstacle for the examination of peptides and proteins that polymerize, and in particular those that form amyloids, is sample preparation. Indeed, the buffer used for the synthesis/purification processes and its composition (counter-ions, mainly chloride ions or trifluoroacetic acid TFA^- ions used for

peptide chemical synthesis) may affect fibrillization [33]. For this reason, batch-to-batch variability of synthetic peptides is frequently reported, resulting in a poor reproducibility of experiments in term of kinetics of self-assembling. Proper storage conditions are also important. Typically, peptides are most stable when stored lyophilized at −20 °C. Nevertheless, even under this condition, hydration occurs. This may affect the presence of pre-formed aggregates in samples. Therefore, in order to ensure comparison between various experiments, we do not recommend storing peptides and proteins for a long time and rather suggest ordering or preparing a fresh batch and performing experiments in a short timeframe.

2. Use of ThT staining is a widely used method and relatively well accepted as an indicator of the presence of amyloid fibrils. Nevertheless, it has to be taken with precaution as ThT can also be an inhibitor of fibrillization [34].
3. A frequently used surface modification protocol for AFM involves fusing unilamelar lipid vesicles on glass or mica to form a supported lipid bilayer that can then be exposed to the protein fibrils. Indeed, interaction of amyloids with membrane is commonly reported and has been observed for Hfq [35, 36].
4. D_2O solutions may be used in samples to avoid the spectral overlaps between the Amide I band and strong absorption band of water at 1640 cm^{-1}. Note that Amide I wavenumbers are lowered in D_20 environment (5–10 cm^{-1}). In this case Amide I/II bands are referred to as Amide I′/II′.
5. The interpretation of an amyloid FTIR spectrum should usually begin with the examination of the primary sequence of the protein/peptide. Indeed, side chains such as asparagine and glutamine, which are very common in amyloid-forming proteins, have IR vibrations that overlap in the Amide I band.

Acknowledgments

This work was supported by Université Paris Diderot, CNRS, CEA, and Synchrotron SOLEIL. We gratefully acknowledge help to MV from the French Embassy for their program for scientific and university cooperation. We are indebted to F. Gobeaux (CEA Saclay, Gif-sur-Yvette, France) and A. Deniset-Besseau (LCP, Université Paris-Sud, France) for many fruitful discussions. We thank Kimberly Stanek (University of Virginia) for her careful and critical reading of our manuscript.

References

1. Taghbalout A, Yang Q, Arluison V (2014) The Escherichia coli RNA processing and degradation machinery is compartmentalized within an organized cellular network. Biochem J 458: 11–22
2. Arluison V, Taghbalout A (2015) Cellular localization of RNA degradation and processing components in Escherichia coli. Methods Mol Biol 1259:87–101
3. Lavelle C, Busi F, Arluison V (2015) Multiple approaches for the investigation of bacterial small regulatory RNAs self-assembly. Methods Mol Biol 1297:21–42
4. Cayrol B, Geinguenaud F, Lacoste J, Busi F, Le Derout J, Pietrement O, Le Cam E, Regnier P, Lavelle C, Arluison V (2009) Auto-assembly of E. coli DsrA small noncoding RNA: molecular characteristics and functional consequences. RNA Biol 6:434–445
5. Busi F, Cayrol B, Lavelle C, LeDerout J, Pietrement O, Le Cam E, Geinguenaud F, Lacoste J, Regnier P, Arluison V (2009) Auto-assembly as a new regulatory mechanism of noncoding RNA. Cell Cycle 8:952–954
6. Vogel J, Luisi BF (2011) Hfq and its constellation of RNA. Nat Rev Microbiol 9:578–589
7. Fischer S, Benz J, Spath B, Maier LK, Straub J, Granzow M, Raabe M, Urlaub H, Hoffmann J, Brutschy B, Allers T, Soppa J, Marchfelder A (2010) The archaeal Lsm protein binds to small RNAs. J Biol Chem 285:34429–34438
8. Smirnov A, Wang C, Drewry LL, Vogel J (2017) Molecular mechanism of mRNA repression in trans by a ProQ-dependent small RNA. EMBO J 36:1029–1045
9. Fortas E, Piccirilli F, Malabirade A, Militello V, Trepout S, Marco S, Taghbalout A, Arluison V (2015) New insight into the structure and function of Hfq C-terminus. Biosci Rep 35:e00190
10. Maury CP (2009) The emerging concept of functional amyloid. J Intern Med 265:329–334
11. Ostrowski A, Mehert A, Prescott A, Kiley TB, Stanley-Wall NR (2011) YuaB functions synergistically with the exopolysaccharide and TasA amyloid fibers to allow biofilm formation by Bacillus subtilis. J Bacteriol 193:4821–4831
12. Zhou Y, Blanco LP, Smith DR, Chapman MR (2012) Bacterial amyloids. Methods Mol Biol 849:303–320
13. Aguilera P, Marcoleta A, Lobos-Ruiz P, Arranz R, Valpuesta JM, Monasterio O, Lagos R (2016) Identification of key amino acid residues modulating intracellular and in vitro microcin E492 amyloid formation. Front Microbiol 7:35
14. Refregiers M, Wien F, Ta HP, Premvardhan L, Bac S, Jamme F, Rouam V, Lagarde B, Polack F, Giorgetta JL, Ricaud JP, Bordessoule M, Giuliani A (2012) DISCO synchrotron-radiation circular-dichroism endstation at SOLEIL. J Synchrotron Radiat 19:831–835
15. Giuliani A, Jamme F, Rouam V, Wien F, Giorgetta JL, Lagarde B, Chubar O, Bac S, Yao I, Rey S, Herbeaux C, Marlats JL, Zerbib D, Polack F, Refregiers M (2009) DISCO: a low-energy multipurpose beamline at synchrotron SOLEIL. J Synchrotron Radiat 16:835–841
16. Wien F, Wallace BA (2005) Calcium fluoride micro cells for synchrotron radiation circular dichroism spectroscopy. Appl Spectrosc 59:1109–1113
17. Lees JG, Smith BR, Wien F, Miles AJ, Wallace BA (2004) CDtool-an integrated software package for circular dichroism spectroscopic data processing, analysis, and archiving. Anal Biochem 332:285–289
18. Micsonai A, Wien F, Kernya L, Lee YH, Goto Y, Refregiers M, Kardos J (2015) Accurate secondary structure prediction and fold recognition for circular dichroism spectroscopy. Proc Natl Acad Sci U S A 112:E3095–E3103
19. Reinke AA, Gestwicki JE (2011) Insight into amyloid structure using chemical probes. Chem Biol Drug Des 77:399–411
20. Rhiannon GC, Christopher TG, Nicolas HV (2012) Characterization of fiber-forming peptides and proteins by means of atomic force microscopy. Curr Protein Pept Sci 13:232–257
21. Dufrene YF, Ando T, Garcia R, Alsteens D, Martinez-Martin D, Engel A, Gerber C, Muller DJ (2017) Imaging modes of atomic force microscopy for application in molecular and cell biology. Nat Nanotechnol 12:295–307
22. Liberelle B, Banquy X, Giasson S (2008) Stability of silanols and grafted alkylsilane monolayers on plasma-activated mica surfaces. Langmuir 24:3280–3288
23. Thompson RF, Walker M, Siebert CA, Muench SP, Ranson NA (2016) An introduction to sample preparation and imaging by cryo-electron microscopy for structural biology. Methods 100:3–15
24. Militello V, Casarino C, Emanuele A, Giostra A, Pullara F, Leone M (2004) Aggregation kinetics of bovine serum albumin studied by FTIR spectroscopy and light scattering. Biophys Chem 107:175–187

25. Byler DM, Susi H (1986) Examination of the secondary structure of proteins by deconvolved FTIR spectra. Biopolymers 25:469–487
26. Zandomeneghi G, Krebs MR, McCammon MG, Fandrich M (2004) FTIR reveals structural differences between native beta-sheet proteins and amyloid fibrils. Protein Sci 13:3314–3321
27. Wallace BA (2009) Protein characterisation by synchrotron radiation circular dichroism spectroscopy. Q Rev Biophys 42:317–370
28. Kardos J, Micsonai A, Pal-Gabor H, Petrik E, Graf L, Kovacs J, Lee YH, Naiki H, Goto Y (2011) Reversible heat-induced dissociation of beta2-microglobulin amyloid fibrils. Biochemistry 50:3211–3220
29. Guinier A (1955) Small-angle scattering of x-rays, Structure of matter series. Wiley, New York
30. Feigin LAS, Svergun DI, Taylor GW (1987) Structure analysis by small-angle X-ray and neutron scattering. Plenum Press, NY, USA
31. Feigin O, Kratky O (1982) Small angle x-ray scattering. Academic Press, New York/London
32. Guinier A (1994) X-ray diffraction: in crystals, imperfect crystals, and amorphous bodies. Courier Corporation, North Chelmsford
33. Kaneko I, Tutumi S (1997) Matters arising: conformations of β-amyloid in solution. J Neurochem 68:438–439
34. Stains CI, Mondal K, Ghosh I (2007) Molecules that target beta-amyloid. ChemMedChem 2:1674–1692
35. Herrera AI, Tomich JM, Prakash O (2016) Membrane interacting peptides: a review. Curr Protein Pept Sci 17:827–841
36. Malabirade A, Morgado-Brajones J, Marquez I, Seguin J, Trepout S, Wien F, Marco S, Velez M, Arluison V (2017) Membrane association of the bacterial riboregulator Hfq and functional perspectives. Sci Rep 7(1):10724
37. Vetri V, D'Amico M, Fodera V, Leone M, Ponzoni A, Sberveglieri G, Militello V (2011) Bovine Serum Albumin protofibril-like aggregates formation: solo but not simple mechanism. Arch Biochem Biophys 508:13–24
38. Vetri V, Militello V (2005) Thermal induced conformational changes involved in the aggregation pathways of beta-lactoglobulin. Biophys Chem 113:83–91
39. Francois-Heude M, Mendez-Ardoy A, Cendret V, Lafite P, Daniellou R, Ortiz Mellet C, Garcia Fernandez JM, Moreau V, Djedaini-Pilard F (2015) Synthesis of high-mannose oligosaccharide analogues through click chemistry: true functional mimics of their natural counterparts against lectins? Chemistry 21:1978–1991